

MHD motion in field-reversed configuration plasma

Taeko IKEYAMA, Masanori HIROI and Yasuyuki NOGI

College of Science and Technology, Nihon University,

Tokyo, Japan

(Received: 1 September 2008 / Accepted: 4 November 2008)

The magnitude of magnetohydrodynamic motion in terms of wobble, internal tilt, external tilt and $n=2$ mode deformation in a field-reversed configuration plasma is quantitatively measured by optical and magnetic methods. In the optical method, a suitable viewing configuration of optical detectors is contrived for each type of motion. In the magnetic method, recently derived analytic formulas are used to obtain the magnitude of the motion from magnetic probe signals. A preliminary result for the quantitative magnitude of each type of motion is reported.

Keywords: field-reversed configuration, FRC, MHD motion, figure-of-eight probe, magnetic probe, bremsstrahlung, wobble, internal tilt, external tilt, rotational instability.

1. Introduction

A field-reversed configuration (FRC) is an elongated compact toroid consisting of only a poloidal field [1-6]. It can confine plasmas with a high value of β , which is the ratio of the plasma pressure p to the magnetic pressure $B_e^2/2\mu_0$, where B_e and μ_0 denote the confinement field outside the plasma and the permeability of free space, respectively. It is possible to attain an average value of β above 0.9 inside a separatrix. The FRC plasma is confined in a strong field produced by a theta-pinch coil. The separatrix radius r_s then becomes smaller than half the coil radius r_w , for example, $r_s/r_w=0.3-0.5$. When the magnetohydrodynamic (MHD) motion of the plasma is discussed, the theta-pinch coil can be replaced by a good conductor. However, the effect of the coil is very weak at small values of r_s/r_w . The above features of the FRC plasma of no toroidal field, high β and small r_s/r_w result in the appearance of many types of MHD motion.

It is known from FRC experiments that the plasma causes various types of MHD motion such as wobble [7], internal tilt [8,9], external tilt [8,10] and $n=2$ mode deformation [11,12] as shown in Fig.1(a). During a wobble, the major axis of the FRC moves in the radial direction with respect to the geometrical axis (z axis) of the theta-pinch coil and rotates randomly around the z axis. The poloidal surfaces of the FRC plasma slide over each other in opposite directions inside the separatrix during an internal tilt. The major axis of the FRC inclines with respect to the z axis during an external tilt. The $n=2$ mode deformation is a transformation of the toroidal surface of the plasma from a circular cross section to a dumbbell cross section. The deformed toroidal surface rotates around the z axis in the direction of the diamagnetic current, which is referred to as a rotational instability [11,12].

However, these types of motion apart from the $n=2$

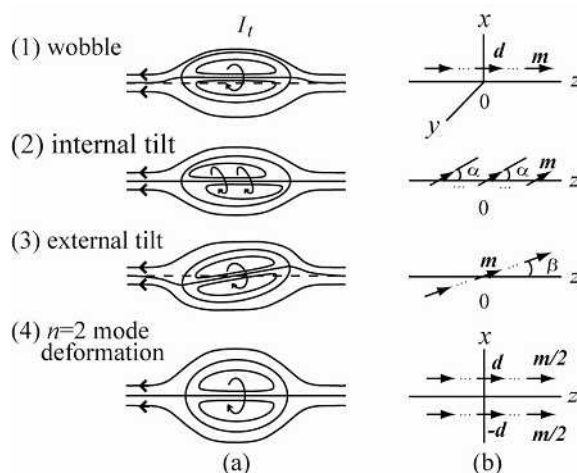


Fig.1 Four types of MHD motion in FRC plasma, which are shown by (a) sketches of field lines on the x - z plane and toroidal current I_t for (1) wobble, (2) internal tilt, (3) external tilt, and $n=2$ deformation, and (b) arrangements of magnetic dipole moments m used to model toroidal current profiles I_t .

mode deformation have been little attention in past experiments for the following two reasons. First, the growth rates of the different types of motions are small. Therefore, they do not have an adverse effect on the confinement of the plasma. Second, the diagnostic systems used to quantitatively measure the magnitudes of the motion are unsatisfactory.

Recently, we have developed two types of diagnostic systems. The first is an optical detector system to measure visible light as shown in Fig.2 [13]. Radiation collected by convex lenses attached to thin optical fibers is sent to optical detectors. The system is constructed with a small size so that it can be easily installed in the narrow space between the theta-pinch coil and a vacuum vessel made of a transparent quartz tube. Therefore, a suitable viewing

T.Ikeyama:taeko@pyxis.phys.cst.nihon-u.ac.jp

configuration of the optical fibers can be arranged for a given type of MHD motion. The second is a magnetic system consisting of a magnetic probe wound in a figure-of-eight shape as shown in Fig.3 [14], and we derived analytic formulas to obtain the magnitudes of the various types of MHD motion using models of magnetic dipole moments \mathbf{m} as shown in Fig.1(b) [15]. The magnetic probe can easily detect a fluctuating axial component of $\tilde{B}_z = 0.1^\circ$ in the confinement field at a given axial position. The various types of MHD motion on the FRC plasma are quantitatively obtained using these new systems and standard FRC diagnostic systems, and typical behaviors of the motions are reported in the present paper.

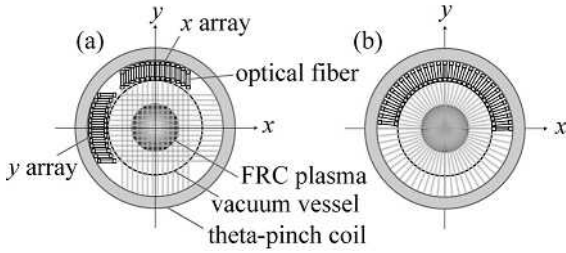


Fig.2 Arrangements of optical fibers in (a) orthogonal viewing configuration and (b) radial viewing configuration.

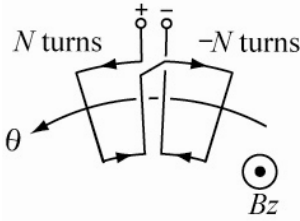


Fig.3 Figure-of-eight wound probe for detecting fluctuating axial field \tilde{B}_z .

2. New diagnostic systems

2.1 Optical detector system

Our constructed diagnostic system consists of a 60-channel set of optical fibers with a flexible viewing configuration [13]. The system can detect radiation from the plasma in the wavelength range of 420-820 nm. Optical filters are used to select the wavelength in the ranges 550 ± 5 nm in the present experiment to observe mainly bramsstrahlung. It is confirmed using a spectroscope that the line radiation from impurity atoms

is at a very low level in this wavelength range.

To measure the wobble and external tilt, two sets of orthogonal viewing configurations of the optical fibers having x and y arrays are installed at $z_{1,2} = \pm 16$ cm as shown in Fig.2(a). Each set has 28 optical fibers. The x and y arrays produce radiation profiles $I(x)$ and $I(y)$, respectively. The center of the $I(x)$ profile moves slightly from $x=0$ to a position x if MHD motion occurs. The $I(y)$ profile moves also from $y=0$ to a position y . As both profiles are measured at two axial positions z_1 and z_2 , the wobble is shown by the time evolution of the following vector on the x - y plane:

$$\mathbf{d}_{\text{opt}} = \left(\frac{x_1 + x_2}{2}, \frac{y_1 + y_2}{2} \right), \quad (1)$$

where subscripts 1 and 2 correspond to z_1 and z_2 , respectively. For the external tilt, the tilt angle β from the z axis shown in Fig.1(b) is

$$\beta = \tan^{-1} \frac{\sqrt{(x_2 - x_1)^2 + (y_2 - y_1)^2}}{z_2 - z_1}. \quad (2)$$

To measure the $n=2$ mode deformation, a radial viewing configuration of the optical fibers is installed at $z=0$ as shown in Fig.2(b), where 28 optical fibers are arranged at 6° intervals. Since the radiation decreases gradually with time due to the loss of plasma, all optical signals are normalized by an average signal $\langle I_j \rangle$ at each moment as

$$I_i^n = \frac{I_i}{\langle I_j \rangle} \left(\langle I_j \rangle = \sum_{j=1}^{28} \frac{I_j}{28} \right), \quad (3)$$

where subscripts i and j denote the optical fiber numbers. Then, Fourier coefficients for the azimuthal mode numbers are calculated from the normalized signals I_i^n . It is noticed that the radial viewing configuration cannot separate motion such the $n=1$ mode as wobble, internal tilt and external tilt, from the $n=2$ mode deformation. Fortunately, it is found in the past study [13] that the sensitivity to the $n=1$ mode motion is very weak compared with that to the $n=2$ mode deformation.

2.2 Magnetic system

The magnetic measurement of the MHD motion has been carried out using a B_θ probe to detect the azimuthal field \tilde{B}_θ [16]. Because the azimuthal field is not included in the confinement field, the detection of \tilde{B}_θ is a conclusive indication of the onset of a type of MHD motion and instability. However, it was found from a recent study that the detection of a small fluctuation of the

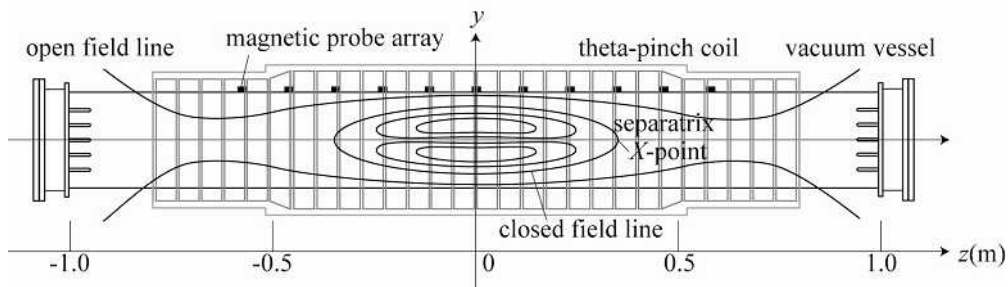


Fig.4 NUCTE-III device and structure of magnetic field lines confining FRC plasma.

axial field \tilde{B}_z is also important for quantitatively estimating the magnitude of MHD motion. Thus, a figure-of-eight wound \tilde{B}_z probe is developed as shown in Fig.3 [14]. As the left-hand-side winding of the probe (N turns) is opposite the right-hand-side winding ($-N$ turns), the uniform confinement field across the windings is cancelled and only a nonuniform axial field \tilde{B}_z is detected.

Both the B_θ and \tilde{B}_z probes are installed azimuthally at 45° intervals around the vacuum vessel in the present experiment to obtain Fourier coefficients for azimuthal mode numbers $n=1$ and 2. The magnitudes of MHD motion are estimated using these Fourier coefficients and the analytic formulas derived in Ref.15.

For the wobble, the radial distance and azimuthal angle on the $r-\theta$ plane are, respectively,

$$d_{\text{mag}} = C_{\text{wob}} r_0 \left(\frac{b^2}{r_w^2} - \frac{1}{2} + \log \frac{r_w}{r_0} \right) \frac{\sqrt{a_{1,z}^2 + b_{1,z}^2}}{|B_{0e}|}, \quad (4)$$

and

$$\theta_{\text{wob}} = \tan^{-1}(b_{1,z} / a_{1,z}). \quad (5)$$

Here, C_{wob} is a correction factor used to adjust errors included in Eq.(4). The radial position of the magnetic probes and the half-length of the separatrix are r_0 and b , respectively. The Fourier coefficients for the $n=1$ mode, $a_{1,z}$ and $b_{1,z}$ are obtained from \tilde{B}_z . The absolute value of the magnetic field, $|B_{0e}|$, is the strength of the axial field at r_0 on the axial midplane of the plasma, excluding that of theta-pinch coil. The azimuthal angle θ_{wob} is measured from the x axis.

For the internal tilt, the tilt angle from the z axis and the azimuthal angle on the $r-\theta$ plane are, respectively,

$$\alpha = \tan^{-1} C_{\text{int}} \left(\frac{2 \left(\frac{b^2}{r_w^2} - \frac{1}{2} + \log \frac{r_w}{r_0} \right) \sqrt{a_{1,\theta}^2 + b_{1,\theta}^2}}{\frac{b^2}{r_0^2} + \frac{1}{2} - \log \frac{2b}{r_0}} \frac{1}{|B_{0e}|} \right), \quad (6)$$

and

$$\theta_{\text{int}} = \tan^{-1}(b_{1,\theta} / a_{1,\theta}) + \frac{\pi}{2}. \quad (7)$$

Here, C_{int} is the correction factor. The Fourier coefficients $a_{1,\theta}$ and $b_{1,\theta}$ are obtained from the B_θ probe signals.

The normalized separatrix radius for the $n=2$ mode deformation is defined as follows:

$$\frac{r_s}{r_{s0}} = \{1 + \xi \cos(2\theta - \delta)\}. \quad (8)$$

Here, r_{s0} is the radius without any deformation, and ξ and δ are the deformation rate and initial phase, respectively. The deformation rate is

$$\xi = C_{\text{def}} \left(\frac{b^2}{r_w^2} - \frac{1}{2} + \log \frac{r_w}{r_0} \right) \frac{r_0^2}{r_{s0}^2} \frac{\sqrt{a_{2,z}^2 + b_{2,z}^2}}{|B_{0e}|}. \quad (9)$$

Here, C_{def} is the correction factor. The Fourier coefficients for the $n=2$ mode, $a_{2,z}$ and $b_{2,z}$, are obtained from \tilde{B}_z . The azimuthal angle at $r_s = r_{s0}(1 + \xi)$ is

$$\theta_{\text{def}} = \frac{1}{2}(\delta + m\pi), \quad (10)$$

where $m = 0, 1, 2$ and $\delta = \tan^{-1}(b_{2,z} / a_{2,z})$.

3. MHD motion

3.1 Experimental setup

The FRC plasmas are produced using deuterium in a NUCTE-III device [5,7] filled to 10 mT pressure as shown in Fig.4, which consists of a vacuum vessel and a theta-pinch coil with length $l_{\text{coil}}=1.5$ m and radius $r_w=17$ cm. The strength of the negative bias field generated by the coil is 32 mT when the confinement field is initiated ($t=0$). The field has a peak of 0.6 T and a 120 μs decay time. The vacuum vessel consists of a transparent quartz tube with radius $r_t=12$ cm. An overview of the behavior of the plasma is shown in Fig.5. The first and second frames show the time evolution of the separatrix radius r_s at the midplane ($z=0$) and the half-length b of the separatrix measured by an excluded flux method, respectively [17].

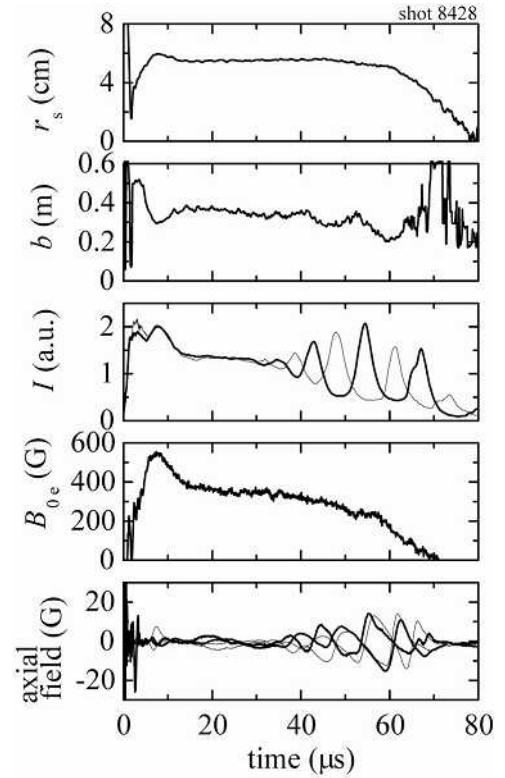


Fig.5 Time evolutions of typical signals obtained from FRC plasma, where the first and second frames are the separatrix radius at $z=0$ and the half-length of the separatrix, respectively. The middle frame is the radiation measured along the x axis (thick line) and y axis (thin line) at a side-viewing slit of the theta-pinch coil. The fourth frame is the magnetic field at $z=0$, excluding that of the theta-pinch coil. The bottom frame shows four signals obtained from the figure-of-eight wound probes.

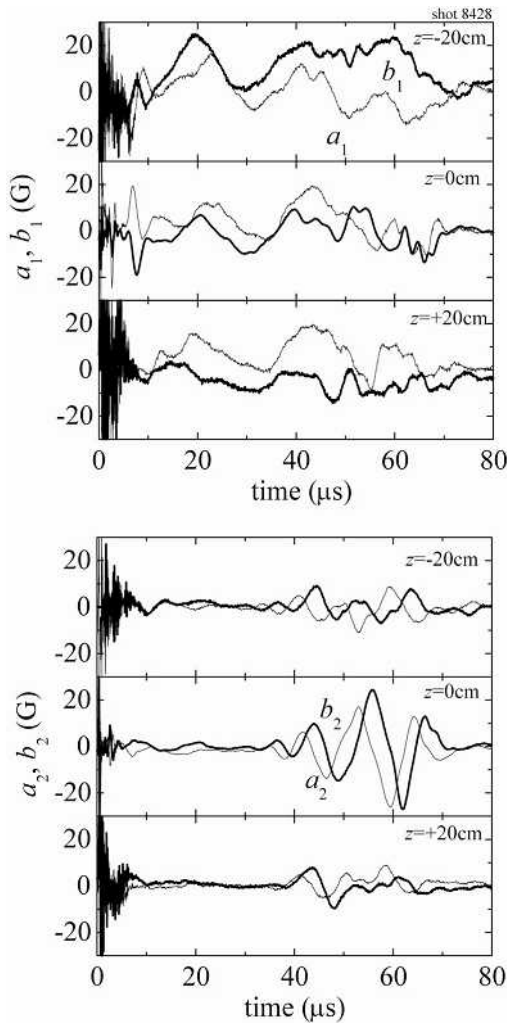


Fig.6 Time evolutions of Fourier coefficients for $n=1$ and $n=2$ modes analyzed from signals of figure-of-eight wound probes at three axial positions.

The radius is $r_s \cong 5.5\text{cm}$ for $t=15\text{--}50\ \mu\text{s}$, although the half-length decreases gradually from $b \cong 40$ to $25\ \text{cm}$. The middle frame shows the radiation measured from a side-viewing slit of the theta-pinch coil at $z = -16\ \text{cm}$. The thick and thin lines show line-integrated radiation along the x and y axes, respectively. The radiation decreases monotonically with time until $t \cong 38\ \mu\text{s}$. After that, the plasma starts to undergo out-of-phase oscillations with increasing amplitude. The oscillations suggest that the plasma with a deformed cross section rotates around the z axis, which causes the onset of the rotational instability. In the fourth frame, the ordinate is B_{0c} at $z=0$. The bottom frame shows four \tilde{B}_z signals generated around the vacuum vessel at equal azimuthal intervals on the axial midplane. The Fourier coefficients for the $n=1$ and 2 modes are obtained from the \tilde{B}_z signals at three axial positions as shown in Fig.6, where the thin and thick lines denote a_n and b_n , respectively. The $n=1$ mode is detected at each time until the end of the discharge, although the $n=2$ mode is only detected after the onset of the rotational instability at $t \cong 38\ \mu\text{s}$.

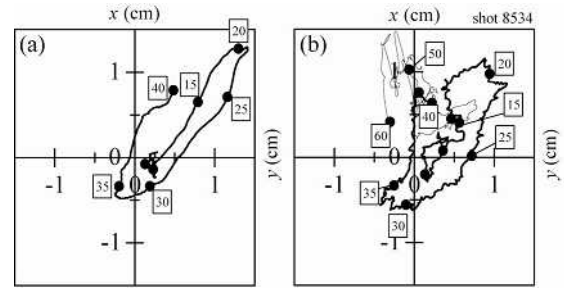


Fig.7 Wobble of plasma on the x - y plane obtained by (a) optical method and (b) magnetic method. The figures in the trajectories denote the times from the start of the confinement field.

3.2 Wobble

When the wobble occurs, the major axis of the FRC is apart from the z axis as shown in Fig.1(b). The position of the major axis on the x - y plane is determined by Eq.(1) for the optical method and by Eq.(4) for the magnetic method. A typical trajectory of the position d_{opt} for $t=5\text{--}40\ \mu\text{s}$ for the former method is shown in Fig.7(a) and that of d_{mag} for $t=5\text{--}60\ \mu\text{s}$ for the latter method is shown in Fig.7(b) where $C_{\text{wob}}=0.67$ is used. The figures in the trajectories denote the times from the start of the confinement field. The observation of d_{opt} is limited to $t=5\text{--}40\ \mu\text{s}$ because the profiles $I(x)$ and $I(y)$ extend beyond the viewing areas of the optical fibers. The trajectory of d_{mag} for $t=5\text{--}40\ \mu\text{s}$ is depicted by a bold line for easy comparison with that of d_{opt} . The motion of the FRC plasma starts at $t \cong 5\ \mu\text{s}$ from near the origin toward the wall of the vacuum vessel and returns to near its initial position after reaching $d_{\text{opt}} \cong 1.8\ \text{cm}$ and $d_{\text{mag}} \cong 1.4\ \text{cm}$ at $t \cong 20\ \mu\text{s}$. It then moves again toward the wall. Both trajectories coincide closely with each other, which means that the motion of plasma particles emitting radiation and toroidal currents flowing in the separatrix are almost the same. The wobble is observed in all FRC plasmas in the present experiment, although the patterns of the trajectories on the x - y plane change on a

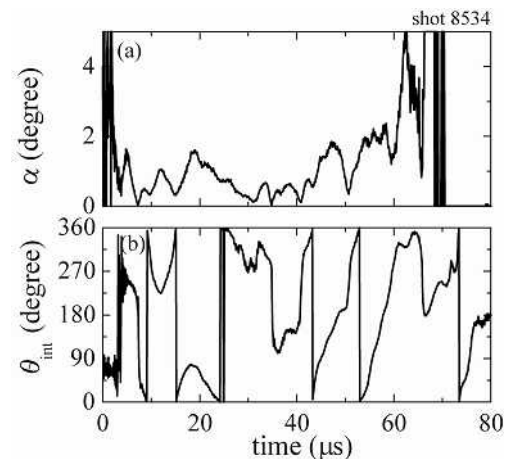


Fig.8 Time evolution of internal tilt angle α from the z axis and azimuthal angle θ_{int} on the r - θ plane obtained by magnetic method.

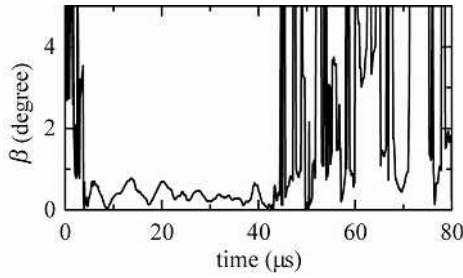


Fig.9 Time evolution of external tilt angle β from the z axis obtained by optical method.

shot-by-shot basis.

3.3 Internal tilt

The internal tilt is only measured by the magnetic method. The time evolution of the tilt angle α obtained from Eq.(6) is shown in Fig.8(a), where $C_{\text{int}}=0.6$ is used. The tilt varies considerably within $\alpha=2^\circ$ for $t=5-40 \mu\text{s}$. The tilt angle shows a tendency to increase with the onset of the rotational instability. The time evolution of θ_{int} in Fig.8(b) clearly shows the rotation of the plasma around the z axis with a period of approximately $10 \mu\text{s}$ during the onset of the rotational instability.

3.4 External tilt

The angle β of the external tilt is estimated by the optical method. The time evolution obtained from Eq.(2) is shown in Fig.9 and the motion becomes noisy after $t \cong 38 \mu\text{s}$ by the same reason explained in 3.2. It is found that β has a small value of less than approximately 0.5° . The value $\beta=0.5^\circ$ corresponds to a radial deviation of $\Delta r=3.5 \text{ mm}$ from the z axis at the separatrix ends (X-points), which is calculated from the relation $\Delta r=b \tan \beta$.

3.5 $n=2$ deformation

Optical signals I_i^n obtained from the radial viewing configuration are shown in Fig.10. The magnitude $I_i^n \cong 1$ for $t=5-38 \mu\text{s}$ denotes the circular cross section of the plasma. After $t=38 \mu\text{s}$, the optical signals oscillate around $I_i^n=1$ owing to the onset of the rotational instability. The deformation rate defined by Eq.(8) is calculated using the Fourier coefficients a_2 and b_2 of I_i^n from the relation $\xi_{\text{opt}} = \sqrt{a_2^2 + b_2^2} / a_0$, where $a_0 = 1/2\pi \sum I_i^n \Delta\theta$. The time evolution of ξ_{opt} is shown in Fig.11 along with the

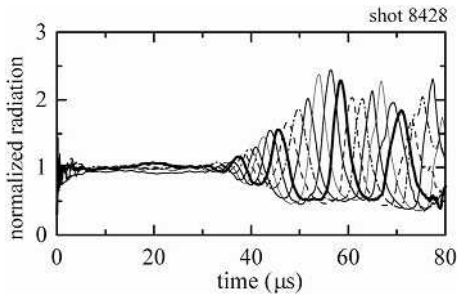


Fig.10 Time evolution of radiation obtained from 8 optical fibers in radial viewing configuration. The radiation is normalized by the average value at each moment.

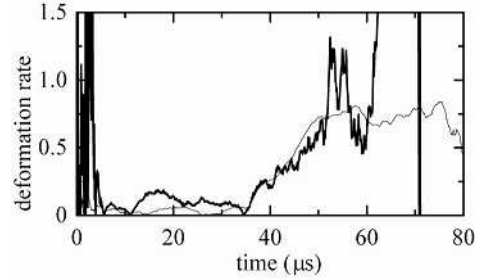


Fig.11 Time evolutions of deformation rate for the $n=2$ mode. The thin and thick lines are obtained by analysis of the optical and magnetic measurements, respectively.

magnetically obtained deformation ξ_{mag} obtained using Eq.(9), where $C_{\text{def}}=0.84$. The values of ξ_{opt} and ξ_{mag} are very small up to $t \cong 38 \mu\text{s}$. They then start to increase linearly in association with the onset of the rotational instability and reach $\xi_{\text{opt}} \cong \xi_{\text{mag}} \cong 0.7$ at $t \cong 50 \mu\text{s}$. Both curves are in close agreement with each other. The azimuthal angle corresponding to the longer axis of the separatrix on the $r-\theta$ plane can be obtained from the optical and magnetic measurements using Eq.(10). The time evolutions of the angles are shown in Fig.12. They are also in good agreement after the onset of the rotational instability, although there is a large error before $t=35 \mu\text{s}$ because of the small amplitude of the $n=2$ mode signals.

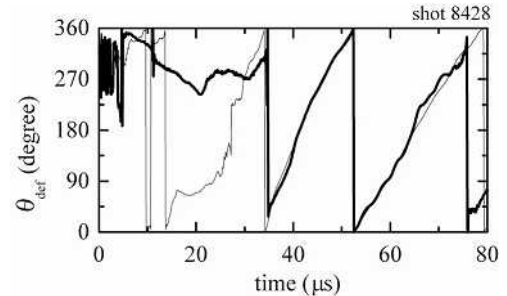


Fig.12 Azimuthal angles of longer axis of separatrix for the $n=2$ deformation on the $r-\theta$ plane. The thin and thick lines are obtained by analysis of the optical and magnetic measurements, respectively.

4. Summary

The magnitudes of the different types of MHD motion in FRC plasmas are quantitatively measured by optical and magnetic methods. A suitable arrangement of optical detectors is contrived for each type of MHD motion, and recently derived analytic formulas for magnetic signals are utilized. It is found that the wobble has a slow oscillation with a period of $30-40 \mu\text{s}$ between the symmetrical axis of the device and the vacuum wall. The internal tilt varies considerably within 2° for $t=5-40 \mu\text{s}$ and becomes large with the onset of the rotational instability. The external tilt can be only observed for $t=5-40 \mu\text{s}$, and it has a smaller

magnitude than the internal tilt during this period. The deformation rate of the plasma cross section is determined by both diagnostic methods. It starts to increase almost linearly with the onset of the rotational instability and reaches approximately 0.7 at $t=50 \mu\text{s}$.

These quantitative analyses of MHD motion will contribute to the study of the onset mechanisms for the motion and the control of its magnitude within a level that does not affect the confinement of the plasma.

- [1] D. J. Rej, W. T. Armstrong, R. E. Chrien, P. L. Klingner, R. K. Linford, K. F. McKenna, E. G. Sherwood, R. E. Siemon, and M. Tuszewski, *Phys. Fluids* **29**, 852 (1986).
- [2] M. Tuszewski, *Nucl. Fusion* **28**, 2033 (1988).
- [3] A. L. Hoffmann and J. T. Slough, *Nucl. Fusion* **33**, 27 (1993).
- [4] H. Himura, S. Okada, S. Sugimoto, and S. Gotô, *Phys. Plasmas* **2**, 191 (1995).
- [5] Y. Ohkuma, M. Urano, M. Nakamura, Y. Narushima, T. Takahashi, and Y. Nogi, *Nucl. Fusion* **38**, 1501 (1998).
- [6] A. L. Hoffmann, P. Gurevick, J. Grossnikle, and J. T. Slough, *Fusion Technol.* **36**, 109 (1999).
- [7] K. Fujimoto, M. Okada, H. Gota, Y. Hasegawa, T. Fujino, T. Asai, T. Takahashi, Y. Nogi, and Y. Ohkuma, *Phys. Plasmas* **12**, 102513 (2005).
- [8] R. Horiuchi and T. Sato, *Phys. Fluids B* **1**, 581 (1989).
- [9] E. V. Belova, S. C. Jardin, H. Ji, M. Yamada, and R. M. Kulsrud, *Phys. Plasmas* **7**, 4996 (2000).
- [10] S. Yoshimura, S. Sugimoto, and S. Okada, *Phys. Plasmas* **14**, 112514 (2007).
- [11] S. Ohi, T. Minato, Y. Kawakami, M. Tanjyo, S. Okada, Y. Itoh, M. Kako, S. Gotô, T. Ishimura, and H. Itô, *Phys. Rev. Lett.* **51**, 1042 (1983).
- [12] S. Shimamura and Y. Nogi, *Fusion Technol.* **9**, 69 (1986).
- [13] T. Takahashi, H. Gota, T. Fujino, M. Okada, T. Asai, K. Fujino, Y. Ohkuma, and Y. Nogi, *Rev. Sci. Instrum.* **75**, 5205 (2004).
- [14] Y. Kanamaru, H. Gota, K. Fujimoto, T. Ikeyama, T. Asai, T. Takahashi, and Y. Nogi, *Rev. Sci. Instrum.* **78**, 036105 (2007).
- [15] T. Ikeyama, M. Hiroi, Y. Nemoto, and Y. Nogi, *Rev. Sci. Instrum.* **79**, 063501 (2008).
- [16] M. Tuszewski, D. P. Taggart, R. E. Chrien, D. J. Rej, R. E. Siemon, and B. L. Wright, *Phys. Fluids B* **3**, 2856 (1991).
- [17] M. Tuszewski, *Rev. Sci. Instrum.* **61**, 2937 (1990).